An Electron Spin−Echo Envelope Modulation (ESEEM) Study of the Q_A Binding Pocket of PS II Reaction Centers from Spinach and *Synechocystis*†

Jeffrey M. Peloquin,‡ Xiao-Song Tang,§ Bruce A. Diner,§ and R. David Britt*,‡

Department of Chemistry, University of California, Davis, Davis, CA, 95616, and Experimental Station, E.I. du Pont de Nemours Company, Wilmington, Delaware 19880-0173

Received August 21, 1998; Revised Manuscript Received November 24, 1998

ABSTRACT: We have used electron spin−echo envelope modulation spectroscopy (ESEEM) to characterize the protein−cofactor interactions present in the Q_A^- binding pocket of PS II centers isolated from spinach and *Synechocystis*. We conclude that the ESEEM spectrum of Q_A^- is the result of interactions of the $S = {}^1/_2$ electron spin of Q_A^- with the $I = 1$ nuclear spins of the peptide nitrogens of two different amino acids. One peptide nitrogen has ESEEM peaks near 0.7, 2.0, 2.85, and 5.0 MHz with isotropic and dipolar hyperfine couplings of $A_{iso} = 2.0$ MHz and $A_{dip} = 0.25$ MHz, respectively. On the basis of these hyperfine couplings we predict the existence of a strong hydrogen bond between Q_A^- and the peptide nitrogen with a hydrogen bond distance of about 2 Å. We have not identified the amino acid origin of this peptide nitrogen. By using amino acid specific isotopic labeling in conjunction with site-directed mutagenesis, we demonstrate that the second peptide nitrogen is that of D2-Ala260, with ESEEM peaks near 0.6 and 1.5 MHz and an isotropic hyperfine coupling, A_{iso}, less than 0.2 MHz. This small isotropic coupling suggests that the D2-Ala260 peptide nitrogen at best forms a weak hydrogen bond with Q_A^-.

Photosystem II of higher plants and cyanobacteria contains two plastoquinone molecules, Q_A and Q_B (*1*). The X-ray structure of the Q_A and Q_B binding pockets in the analogous non-oxygen-evolving purple bacterial photosynthetic reaction center indicates that Q_A may form hydrogen bonds with residues M-His219 and M-Ala260 and Q_B may form hydrogen bonds with L-His190 and L-Ser223 (*2*, *3*). It has been proposed that similar interactions exist in PS II[1] centers between Q_A and residues D2-His215 and D2-Ala260 and Q_B to D1-His215 and D1-Ser264 (*2*−*4*). Figure 1 shows a model of the binding site. The residues D1-His215 and D2-His215 (spinach numbering) are also proposed to be ligands to the non-heme iron, which lies between Q_A and Q_B. ESEEM, ENDOR, CW-EPR, and FT-IR spectroscopies have been used to characterize the hydrogen bond interactions between the protein and Q_A^- in bacterial and PS II photosynthetic systems (*5*−*19*). FT-IR (*5*, *6*) and Q-band CW-EPR (*7*) experiments on bacterial reaction centers demonstrate that the O4 oxygen of Q_A^- does indeed form a strong hydrogen bond, presumably to M-His219, but that the O1 oxygen does not participate in a hydrogen bond. The same FT-IR (*5*, *6*) and Q-band CW-EPR (*7*) studies indicate that there are hydrogen bonds to the O1 and O4 oxygens of Q_B^- and these bonds are of equal strength.

The presence of these hydrogen bonds should place any potential hydrogen bond donor close enough to Q_A^- to produce a magnetic coupling of the $S = {}^1/_2$ electron spin of Q_A^- with the $I = 1$ nuclear spin of any hydrogen bonded nitrogens (e.g. the peptide and imidazole nitrogens of D2-Ala260 and D2-His215, respectively). Over the past two years a number of groups have used electron spin−echo envelope modulation (ESEEM) spectroscopy to study the magnetic couplings of Q_A^- to nearby nitrogen nuclei in both PS II and photosynthetic bacterial samples (*8*−*13*). Unfortunately, the electron spin ($S = 2$) of the non-heme iron situated between Q_A and Q_B is magnetically coupled to the electron spin of Q_A^-, leading to a broadening of the Q_A^- EPR signal and prohibitory fast spin relaxations processes (*14*, *15*, *20*). As a result, to perform ESEEM spectroscopy on Q_A^-, it has previously been necessary to decouple the spin of the non-heme iron from the spin of Q_A^-. There have been two common methods to perform this decoupling: the

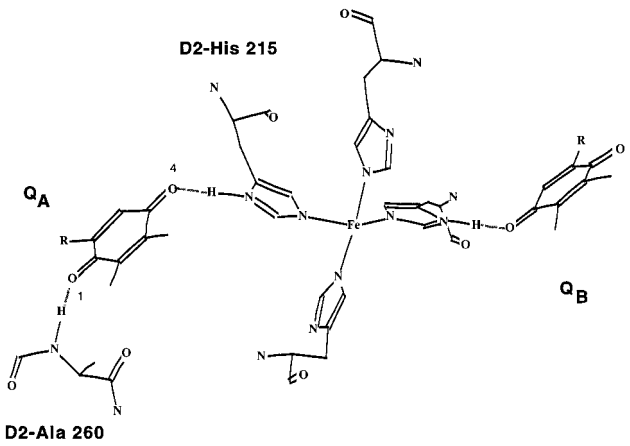

FIGURE 1: Model of the Q_A binding site in PS II based on the Q_A binding site in *Rb. sphaeroides* (*2*) showing the proposed hydrogen bonds between and D2-His215 and D2-Ala260.

† Support provided by NSF (MCB 9513648) to R.D.B. and by NRICGP/USDA (94-37306-0783) to B.A.D.

‡ University of California, Davis.

§ E.I. du Pont de Nemours Company.

[1] Abbreviations: ESEEM, electron spin echo envelope modulation; 2P-FT-ESEEM, two-pulse Fourier transform electron spin echo envelope modulation; 3P-FT-ESEEM, three-pulse Fourier transform electron spin echo envelope modulation; ENDOR, electron nuclear double resonance; PS II, photosystem II.

10.1021/bi982033l CCC: $18.00
Published on Web 01/29/1999

Table 1: Comparison of the ESEEM Peaks Assigned to a Peptide Nitrogen and a Histidine Nitrogen in Spinach PS II BBY Centers and in *Rhodobacter sphaeroides* Reaction Centers

$Zn\text{-}Q_A^-$	peptide (MHz)	histidine (MHz)	ref
spinach BBY	0.88, 2.02, 2.88, 5.0	0.53, 0.88, 1.46, 4.3	*9*
Rb. sphaeroides	1.0, 1.8, 2.78, 4.2	0.64, 0.85, 1.46, 4.2	*10*

actual removal of the non-heme iron and its replacement with the diamagnetic ion, Zn^{2+} (*9*−*11*, *14*), or treatment of PS II centers with CN^- which leads to the conversion of the non-heme iron to its low-spin form ($S = 0$) (*21*). It is not known to what extent either decoupling treatment alters the interactions of Q_A^- with its surroundings.

Astashkin et al. (*9*) used ESEEM to examine Q_A^- in Zn-substituted spinach PS II membranes and interpreted their data as evidence that Q_A^- is coupled to a peptide nitrogen as well as an imidazole nitrogen of a histidine (see Table 1). On the basis of the proposed structural homology between PS II and bacterial reaction centers (*2*, *4*, *22*), they assigned the peptide and histidine nitrogens to the residues D2-Ala260 and D2-His215. MacMillan et al. have also reported similar data (*13*). As for the actual bacterial centers, Spoyalov et al. (*10*) used ESEEM to characterize Q_A^- in Zn-substituted bacterial reaction centers and observed ESEEM peaks consistent with Q_A^- being coupled to a peptide nitrogen as well as a histidine nitrogen (see Table 1).

Kawamori et al. (*16*) and MacMillan et al. (*13*) have also studied Q_A^- in CN-treated PS II membranes using ESEEM spectroscopy. While they observed the Q_A^-−peptide nitrogen coupling, they saw no evidence for a coupling to a histidine nitrogen. They proposed that the CN^- ligation to the non-heme iron leads to the displacement of the D2-His215 and the subsequent loss of the Q_A^-−histidine nitrogen coupling.

Deligiannakis et al. (*8*) have also recorded the ESEEM spectra of Q_A^- in CN-treated ^{14}N-natural abundance spinach PSII membranes as well as in globally ^{15}N-labeled spinach PS II membranes and report only a coupling between Q_A^- and a peptide nitrogen. Deligiannakis et al. (*17*) studied the effects of high pH on the ESEEM spectrum of Q_A^-. At pH 11, without the addition of CN^-, they observed a decoupling of the electron spins of the non-heme iron and Q_A^-, that is, a recovery of the narrow EPR signal at $g = 2$ characteristic of Q_A^-. In this case, they do predict a coupling between Q_A^- and histidine in addition to the coupling between Q_A^- and a peptide nitrogen.

Although researchers in these previous papers proposed specific amino acid assignments for the various peaks in the ESEEM spectra of Q_A^- in PSII, they provided no direct experimental evidence for these assignments. Such specific assignments require a combination of isotopic labeling of individual amino acids and site-directed mutagenesis. We showed previously (*12*) that the non-heme iron and Q_A^- spins were decoupled in PS II centers isolated from *Synechocystis* using a hydroxylapatite column. We reported ESEEM spectra of Q_A^- in CN-treated PS II centers isolated from *Synechocystis* at pH 9.2 and 7.8 and the ESEEM spectrum of Q_A^- in non-CN-treated PS II centers at pH 7.8. At pH 7.8, in addition to PS II centers with natural abundance nuclei, we examined PS II centers that were globally labeled with ^{15}N and PS II centers in which all of the nitrogen nuclei were ^{15}N-labeled except for the imidazole and peptide nitrogens of histidine residues. These isotopic labeling experiments clearly demonstrated that there was no observable contribution to the ESEEM spectrum from histidine nitrogens. This result is consistent with the results of ESEEM experiments on CN-treated spinach PS II centers discussed above.

In this paper, we present the results of a series of experiments designed to better characterize the magnetic interactions between Q_A^- and nearby nitrogen nuclei. We present, for the first time, the ESEEM spectra of Q_A^- in spinach PS II centers in which the non-heme iron is in its native high spin state and coupled to the electron spin of Q_A^-. These spectra allow us to determine the extent to which the two methods of decoupling the quinone spin from that of the iron spin perturb the magnetic interactions of the quinone with its surroundings. We then present the ESEEM spectra of Q_A^- in CN-treated and Zn-substituted spinach PS II centers (pH 8.0) at two different values of the applied magnetic field. We also present the ESEEM spectrum of Q_A^- in CN-treated PS II membranes at pH 6.0 and 10.0. Last, we present the ESEEM spectra of Q_A^- in a series of isotopically labeled PS II centers isolated from wild type and site-directed mutants of the cyanobacterium *Synechocystis*. These isotopic labeling experiments provide a concrete basis for re-evaluating the previous assignments of the Q_A^- ESEEM spectra.

MATERIALS AND METHODS

Isolation of Spinach "BBY" Membranes. PS II oxygen-evolving membranes were prepared from market spinach using a slightly modified version of the BBY preparation (*23*) as described by Campbell et al. (*24*). These membranes were then incubated in 0.8 M Tris (pH 8.0) for 30 min at 0 °C in room light to disrupt the manganese cluster of the oxygen-evolving complex. Cyanide treatment was performed using the method of Sanakis et al. (*21*). Fe-depletion and Zn-substitution followed the method of Klimov et al. (*14*) and Astashkin et al. (*9*). In all cases the final pellet was resuspended in 5 mM $MgCl_2$, 15 mM NaCl, 5 mM $CaCl_2$, and 1 mM EDTA. For pH 6.0, 8.0, and 10.0, 50 mM MES, 50 mM HEPES, and 50 mM glycine, respectively, were used. Fifty millimolar sodium dithionite (final concentration) was added to each sample, except where noted, to reduce Q_A to Q_A^-. The samples were then loaded into EPR tubes and frozen in liquid nitrogen. All of the above processes were performed in dim light.

Isolation of Synechocystis Core Particles. Mutant and wild-type strains of the glucose-tolerant strain of *Synechocystis* PCC 6803 were grown photoheterotrophically as described earlier (*25*). For ^{15}N-global labeling experiments the sole source of nitrogen was $Na^{15}NO_3$ (>98%, Cambridge Isotope) at a concentration of 3 mM in BG-11 medium (*26*) containing 5 mM glucose. To obtain cells containing ^{14}N-histidine in an ^{15}N background, the cells of the histidine-tolerant strain of *Synechocystis* were grown photoautotrophically in BG-11 medium where the only nitrogen sources were 3 mM $Na^{15}NO_3$ plus 120 μM L-^{14}N-histidine. Under these experimental conditions, 85% of the histidine molecules incorporated into the reaction centers were from the histidine supplied in the growth medium as shown previously by mass spectral analysis of histidine in hydrolyzed PSII centers (*27*).

To obtain cells containing ^{15}N-alanine or ^{15}N-glycine, we grew the cells photoautotrophically in BG-11 medium

containing 0.5 mM ^{15}N-alanine or ^{15}N-glycine. In experiments with ^{13}C-alanine labeling (unpublished), protein hydrolysis, HPLC, and mass spectral analysis indicated that 70% of the alanine incorporated into the thylakoid membranes was from the alanine supplied in the growth medium. These results imply that the added alanine is directly incorporated into protein, competing favorably with endogenous alanine production and with little equilibration with cellular pools of pyruvate.

PSII core complexes were isolated as described by Tang and Diner (*25*) followed by hydroxylapatite column chromatography as described by Rögner et al. (*28*). The PSII core complexes were passed through a desalting column (Econo Pac 10 DG, BioRad) equilibrated with 50 mM Tricine-NaOH (pH 7.8) containing 0.4 M sucrose, 15 mM NaCl, and 5 mM $MgCl_2$ and concentrated overnight at 4 °C. Alternatively, PSII core complexes were desalted in 50 mM MES−NaOH, pH 6.0, 25% glycerol (w/v), 20 mM $CaCl_2$, and 5 mM $MgCl_2$ and stored at −80 °C (*27*). They were subsequently exchanged into Tricine buffer and subjected to cyanide treatment according to Sanakis et al. (*21*) with some modification (*29*).

EPR Experiments. The electron spin−echo envelope modulation experiments (ESEEM) were performed with an instrument of our own design and construction (*30*). The two-pulse ESEEM ($\pi/2$-τ-π-τ-ESE) data were collected by incrementing the time τ between the first and second microwave pulses. The three-pulse ESEEM ($\pi/2$-τ-$\pi/2$-T-$\pi/2$-τ-ESE) data utilized a constant interpulse time τ, chosen to suppress proton modulation, while incrementing the time T between the second and third microwave pulses. The frequency domain spectra of all ESEEM patterns are shown in the form of a cosine Fourier transform. The time domain data within the instrumental dead time were reconstructed with a cosine Fourier backfill method (*31*). All experiments on uncoupled Fe-Q_A^- were conducted at 20 K. The repetition delay time between successive microwave pulse sequences was set at 20 ms in the ESEEM experiments. Experiments on the untreated Fe-intact spinach PS II centers in which the Fe and quinone spins are coupled were performed at a temperature of 1.4 K and at a repetition rate of 2 ms. Except where noted all experiments were carried out at pH 8.0.

Fluorescence Experiments on D2-Ala260 and D2-Trp253 Mutants. For measurements of fluorescence relaxation, the concentration of whole *Synechocystis* cells was adjusted to 0.9 OD at 730 nm with BG-11 medium and treated for 10 min in the dark with 0.3 mM *p*-benzoquinone plus 0.3 mM $K_3Fe(CN)_6$. The flash detection spectrophotometer used for these experiments has been described previously (*32*). Two types of fluorescence experiments were performed. The rate of Q_A to Q_B electron transfer was analyzed using actinic xenon flashes given every 600 ms and followed by a train of detecting flashes to monitor the fluorescence yield. As there is little energy transfer between centers in *Synechocystis*, the fluorescence yield is a direct indicator of the concentration of Q_A^-. The rate of charge recombination between Q_A^- and the electron donor side was monitored using similar detecting flashes following a single actinic flash in cells treated with 40 μM DCMU.

To characterize the extent to which the D2-Ala260 to Gly mutation affects the Q_A binding pocket, we measured the rate of electron transfer from Q_A to Q_B/Q_B^- by monitoring the relaxation of the yield of fluorescence following each of five actinic flashes. The rate of oxidation in the mutant ($t_{1/2}$ = 0.2 ms) is similar to that of wild type ($t_{1/2}$ = 0.13 ms) and oscillates with a periodicity of two, faster on odd than on even numbered flashes. These experiments clearly show that the mutation D2-Ala260 to Gly does not alter the rate of electron transfer between Q_A and Q_B.

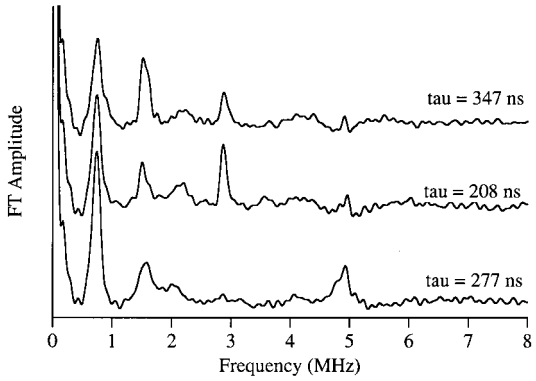

FIGURE 2: Three-pulse ESEEM Fourier transform spectra of Q_A^- in Fe-intact, spinach BBY PS II membranes. Experimental conditions: ν = 9.2463 GHz, microwave paper 50 W, $\pi/2$ pulse = 10 ns, H = 3390 G, T = 1.4 K.

We also measured the change in the yield of fluorescence of PS II centers containing DCMU which binds to the pocket and prevents electron transfer between Q_A and Q_B. The change in yield of fluorescence following a single actinic flash represents the rate of charge recombination between Q_A^- and the donor side of PS II. It is clear that the D2-Ala260 to Gly mutation ($t_{1/2}$ = 13 s) results in a decrease in the rate of charge recombination relative to the wild type ($t_{1/2}$ = 0.76 s). This experiment suggests that the D2-Ala260 to Gly mutation results in some energetic stablization of Q_A^-.

We also used fluorescence spectroscopy to determine the rate of electron transfer between Q_A^- and Q_B/Q_B^- in *Synechocystis* centers in which D2-Trp253 has been mutated to phenylalanine or tyrosine. These experiments show that the D2-Trp253 to Tyr mutation (biexponential with $t_{1/2}$ = 0.24 ms (65%) and $t_{1/2}$ = 2.7 ms (35%)) results in a decrease in the rate of electron transfer from Q_A to Q_B while the D2-Trp253 to Phe mutant is similar to wild type. Fluorescence experiments on DCMU containing *Synechocystis* centers clearly show that the D2-Trp253 to Tyr mutation ($t_{1/2}$ = 14 s) results in a decrease in the rate of charge recombination between Q_A^- and the donor side of PS II, while the D2-Trp253 to Phe is similar to wild type ($t_{1/2}$ = 0.76 s). As with the D2-Ala260 to Gly mutation, we conclude that the D2-Trp253 to Tyr mutation results in a slight energetic stabilization of Q_A^- while the D2-Trp253 to Phe is indistinguishable from wild type.

RESULTS

Spinach BBY PS II Membranes. To alleviate the problems associated with the fast relaxation processes of the Fe-Q_A^- system, we have performed ESEEM experiments at the very low temperature of 1.4 K. Figure 2 shows the three-pulse FT-ESEEM spectra of the coupled Fe-Q_A^- radical in tris-washed dithionite-reduced PS II membranes at 1.4 K. To observe all possible ESEEM peaks, we collected the ESEEM spectra at three different separations, τ, of the pulses 1 and

Table 2: Comparison of the ESEEM Peaks Assigned to the N_X and N_Y Nitrogens Coupled to Q_A^-

sample	N_X (MHz)	N_Y (MHz)
spinach[a]		
Fe-Q_A^-	0.75, 2.0-2.2, 2.86, 4.95	1.57
CN-Fe-Q_A^- (3306 G)	0.75, 2.07, 2.85, 4.4-5.0	1.58
CN-FeQ_A^- (3905 G)	0.75, 2.07, 2.85, 4.96-5.35	1.58
CN-Fe-Q_A^- (pH 10)	0.75, 2.07, 2.85, 4.4-5.0	1.58
CN-Fe-Q_A^- (pH 6)	0.75, 2.07, 2.85, 4.4-4.7	1.46
Zn-Q_A^- (3306 G)	0.75, 2.08, 2.87, 4.3-4.7	(0.6?), 1.46
Zn-Q_A^- (3905 G)	0.75, 2.08, 2.87, 4.74-5.0	(0.6?), 1.46
Synechocystis[b]		
CN-Fe-Q_A^- (pH 9.2)	0.7, 2.0, 2.85, 4.4-5.0	1.55
CN-Fe-Q_A^- (pH 7.8)	0.7, 2.0, 2.85, 4.4-5.0	1.51
Fe-Q_A^- (pH 7.8)[c]	0.7, 2.0, 2.85, 4.4-5.0	0.6, 1.47, 2.2
CN-Fe-Q_A^- (pH 6)	0.7, 2.0, 2.85, 4.4-5.0	1.52
CN-Fe-Q_A^- (^{15}N labeled)	0.28, 2.8	1.46
Fe-Q_A^- (D2-A260G)[c]	0.8, 2.0, 2.85, 4.4-5.0	0.65, 1.46, 2.2

[a] All samples are pH 8 unless otherwise indicated. [b] All samples were were purified using a hydroxylapatite column. [c] No cyanide was added to this sample. The use of a hydroxylapatite column during purification leads to a decoupling of the Fe and quinone electron spins.

2 in the three-pulse ESEEM sequence. Together, the three τ values in Figure 2 reveal 5 ESEEM peaks at frequencies of 0.75, 1.57, 2.0−2.2, 2.86, and 4.95 MHz (See Table 2). No ESEEM peaks were detected in spinach PS II membranes which had not been dithionite-treated. It is thus reasonable to assign the observed peaks to the nuclear transition frequencies of magnetic nuclei coupled to the Fe-Q_A^- spin center. The 0.75, 2.0−2.2, 2.86, and 4.95 MHz peaks are quite similar to the peaks which were assigned previously to a peptide nitrogen in reaction centers in which the iron was magnetically uncoupled from the quinone (*8*, *9*, *12*, *13*).

One potential problem with our assignment is, since we are looking at a coupled system, the observed ESEEM peaks may arise from the histidine ligands to the non-heme iron. However, the frequencies of the Fe electron spin transitions, ν(Fe), are significantly different from the frequencies of the Q_A^- electron spin transition, $\nu(Q_A^-)$. Although the coupling between the Fe and Q_A^-, J(Fe-Q_A^-), is strong enough to distort the magnetic properties of Q_A^-, the coupling is significantly smaller than the difference in the electron spin transition frequencies of the Fe and Q_A^-, $J(\text{Fe-}Q_A^-) \ll \Delta(\nu(\text{Fe}) - \nu(Q_A^-))$ (*20*). As a result, the ESEEM data in Figure 2 contain no contribution from nuclei magnetically coupled to the non-heme iron.

Figure 3 shows the 3P−FT-ESEEM spectra of Q_A^- in CN-treated spinach PS II centers at two different magnetic fields (Figure 3A, 3306 G, and Figure 3B, 3905 G) and three different values of τ, the spacing between the first and second microwave pulses of the pulse sequence. In Figure 3A, peaks are present at 0.75, 1.58, 2.07, 2.85, and 3.65 MHz in all three traces. The relative intensities of the different peaks display a marked dependence on the choice of τ. Such dependencies are highly useful in comparing 3P-FT-ESEEM spectra of different samples. If two different samples (e.g., CN-treated PSII versus Zn-substituted PS II) have ESEEM peaks with similar frequencies whose intensities have a similar dependence on τ, it is reasonable to assign the ESEEM spectra to the same nucleus in both cases. We will be using this idea throughout this paper in our discussion of ESEEM peaks near 1.5 and 5.0 MHz.

Also present in Figure 3 is a feature near 5.0 MHz whose exact frequency depends on the choice of τ. This feature

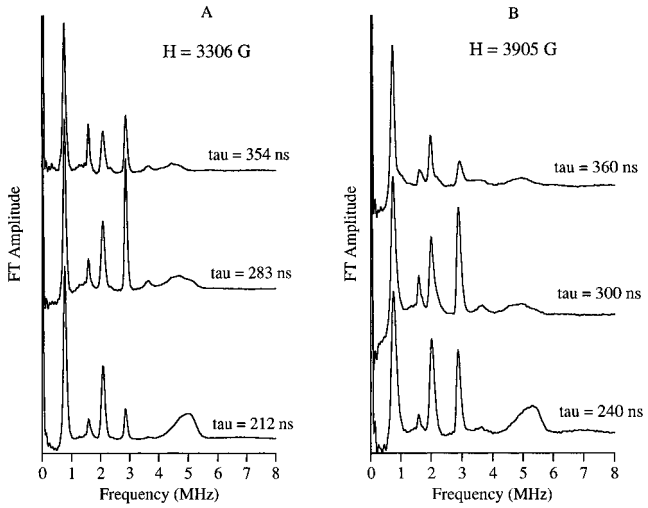

FIGURE 3: Three-pulse ESEEM Fourier transform spectra of Q_A^- in spinach BBY PS II membranes treated with 340 mM NaCN for 1.5 h: (A) $\nu = 9.26$ GHz, $H = 3306$ G; (B) $\nu = 10.950$ GHz, $H = 3905$ G. For both A and B, microwave paper 50 W, $\pi/2$ pulse = 10 ns, and $T = 20$ K.

has frequencies of 4.43, 4.70, and 5.00 MHz for $\tau = 354$, 283, and 212 ns, respectively. A single broad peak is present at 5.00 MHz in the 2P-FT-ESEEM spectrum (data not shown). These spectra are consistent with those reported previously by Deligiannakis et al. (*8*). Figure 3B shows that an increase of the applied microwave frequency and external field (while maintaining a constant g factor) leads to a change in the frequency of only this 4−5 MHz peak. For $H = 3906$ G, the frequencies are 4.96, 4.96, and 5.35 MHz at $\tau = 360$, 300, and 240 ns, respectively, and 5.3 MHz (2P−FT-ESEEM spectrum, data not shown).

In a system with natural abundance levels of nuclear isotopes, the observation of nuclear transition frequencies in the 1−6 MHz region suggests a coupling between an electron spin and a nearby ^{14}N nucleus. If the strength of the applied magnetic field is chosen such that the nuclear Larmor frequency of a nitrogen of interest is equal to approximately one-half of the isotropic electron−nuclear hyperfine coupling constant, then, for one of the electron spin manifolds, the Zeeman and hyperfine terms of the spin Hamiltonian are of equal but opposite magnitude and as a result their respective contributions to the spin Hamiltonian cancel and the nuclear transition frequencies for this electron spin manifold are determined solely by the electric-quadrupole interaction. Since this latter interaction is independent of the applied magnetic field orientation and strength, the corresponding ESEEM peaks are quite intense and narrow. This situation is termed the "exact field cancellation" condition, due to the mutual cancellation of the Zeeman and hyperfine terms at a particular magnetic field strength (*33*).

For this canceling manifold, the frequencies of the ESEEM peaks are given by the relations

$$\nu_o = \frac{2\eta e^2 qQ}{4}, \quad \nu_- = \frac{e^2 qQ(3-\eta)}{4}, \quad \nu_+ = \frac{e^2 qQ(3+\eta)}{4} \tag{1}$$

where Q is the nuclear quadrupole moment of an ^{14}N nucleus; q is the z-component of electric field gradient across the nucleus; η is the asymmetry parameter which describes the

x- and *y*-components of the electric field gradient across the nucleus; and *e* is the electron charge. From eq 1, it can be seen that the frequency of ν_+ equals the sum of the ν_o and ν_- frequencies. For ESEEM spectra containing contributions from many nuclei, this sum rule is of great utility for identifying ESEEM peaks of a particular nucleus.

In accordance with previous ESEEM studies of Q_A^-, we assign the 0.75, 2.07, and 2.85 MHz peaks to the transitions of a single nitrogen, which we term N_X. By using eq 1, we calculate $e^2qQ = 3.22$ MHz and $\eta = 0.51$. These quadrupole parameters are consistent with N_X being a peptide nitrogen of an amino acid residue in the vicinity of Q_A^- (*34*). The 1.58 MHz peak then represents a second nitrogen nucleus magnetically coupled to Q_A^- which we will refer for the time being as N_Y but will assign to a particular amino acid residue later in the paper.

Two small peaks are present in Figure 3, parts A and B, at frequencies of about 2.2 and 3.6 MHz. If two or more nuclei are coupled to an electron spin, ESEEM combination peaks will be present at the sum and difference of the individual ESEEM peaks of the two nuclei. For example, the 2.2 MHz peak would be the sum combination peak of the 0.75 MHz peak of N_X and the 1.55 MHz peak of N_Y. Likewise the 3.6 MHz peak would be the combination peak of the 1.55 MHz peak of N_Y with the 2.0 MHz peak of N_X. If this assignment is correct, it demonstrates that N_X and N_Y are both coupled to Q_A^- in some fraction of the PS II centers.

In the noncancellation manifold, near exact field cancellation conditions, only the $\Delta m_I = 2$ transition, the so-called double quantum transition, will typically give rise to a detectable ESEEM peak (*33*). The maximum of this peak is given approximately by the relation

$$\nu_{dq} = \sqrt{4\left[\left(\nu_N \pm \frac{A_{iso}}{2}\right)^2 + \left(\frac{e^2qQ}{4h}\right)^2(3+\eta^2)\right]} \qquad (2)$$

where A_{iso} is the isotropic hyperfine coupling constant between the ^{14}N nitrogen and the $S = {}^1/_2$ electron spin and ν_N is the nuclear Larmor frequency of ^{14}N.

The dependence of the peak on the Larmor frequency of ^{14}N indicates that the frequency of ν_{dq} will depend on the strength of the applied magnetic field. The only field-dependent peak in Figure 3 is the 4−5 MHz peak. With the use of the 5.0 MHz value from the 2P-ESEEM spectra (data not shown), eq 2 would predict that for the N_X nitrogen, A_{iso} is about 1.8 MHz. At a field of 3302 G, the Larmor frequency of ^{14}N is 1.02 MHz. It is thus clear that A_{iso} of N_X is close to twice the Larmor frequency and is near the exact field cancellation condition.

Our assignment of the nitrogen as a peptide nitrogen near exact field cancellation with hyperfine and quadrupole parameters of $A_{iso} = 1.8$ MHz, $e^2qQ = 3.2$ MHz, and $\eta = 0.5$ is consistent with previous assignments by Deligiannakis et al. (*8*). The observed shift in the frequency of ν_{dq} with τ was also observed by Deligiannakis et al. (*8*) and assigned to a splitting of the ν_{dq} peak of the peptide nitrogen. Such splitting can occur for nuclei near exact field cancellation if η is greater than zero (*33*). Therefore, we conclude, as did Deligiannakis et al., that the 4.43 MHz peak is part of the ESEEM line shape of the ν_{dq} transition of N_X and not a nuclear transition frequency of a different nitrogen nucleus.

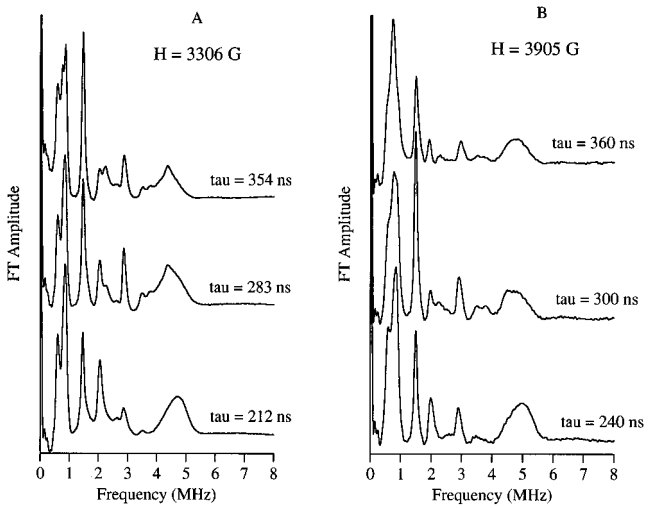

FIGURE 4: Three-pulse ESEEM Fourier transform spectra of Q_A^- in spinach BBY PS II centers in which the non-heme iron is replaced with zinc: (A) $\nu = 9.26$ GHz, $H = 3306$ G; (B) $\nu = 10.95$ GHz, $H = 3905$ G. For both A and B, microwave paper 50 W, $\pi/2$ pulse = 10 ns, and $T = 20$ K.

A more severe method for decoupling of the non-heme iron and Q_A^- electron spins is through the actual removal of the non-heme iron and its replacement with zinc. Figure 4 shows the 3P-FT-ESEEM spectra of Zn-Q_A^- at two different fields (Figure 4A, 3306 G and Figure 4B, 3905 G) and three different values of τ. Field-independent peaks are present at 0.58, 0.75, 0.85, 1.46, 2.08, 2.2, 2.6, 2.87, and 3.6 MHz. In Figure 4A, a τ-dependent peak is present at 4.30 and 4.72 MHz for $\tau = 354$ and 212 ns, respectively. An increase of the applied microwave frequency and external field (while maintaining a constant *g* factor) to 3905 G leads to τ-dependent peaks at 4.74 and 5.0 MHz (Figure 4B). Two-pulse ESEEM data also show a single field-dependent peak at 4.35 and 5.0 MHz for $H = 3306$ and 3905 G (data not shown).

Although there are large changes in the ESEEM spectra between Figures 3 and 4, it is reasonable to propose that the Q_A^-−N_X peptide nitrogen coupling still exists and to assign the 0.75, 2.08, and 2.87 MHz peaks to the N_X-peptide nitrogen. While there is a change in the intensity of the 4−5 MHz peaks, Figure 4 shows the same dependence on the choice of τ as do the 4−5 MHz peaks in Figure 3. This similarity suggests that the τ and field-dependent 4−5 MHz peaks in Figure 4 can be assigned to the ν_{dq} transition of the N_X peptide nitrogen. From eq 2, the decrease in the frequency ν_{dq} upon Zn repletion would indicate a 0.5 to 0.7 MHz decrease in the coupling between Q_A^- and N_X upon Fe depletion and Zn substitution.

Examination of Figures 3 and 4 shows that the intensity of the 1.46 MHz peak in Figure 4 has the same dependence on τ as does the intensity of the 1.58 MHz peak in Figure 3, which we assigned to the coupling of Q_A^- with the nitrogen, N_Y. As a result, we propose that the 1.46 MHz ESEEM peak in Figure 4 is evidence that Q_A^- is coupled to this same nitrogen in Zn-substituted spinach PS II membranes. However, it is clear that the relative intensity of the 1.46 MHz peak in Figure 4 is significantly larger than in Figure 3. Normalization of the data in Figures 3 and 4 shows that the intensity of the ESEEM peaks of N_X are approximately 50% larger for the CN-treated spinach PS II membranes (Figure

3) than for the Zn-substituted spinach PS II membranes (Figure 4). This normalization also shows that the 1.46 MHz peak in Figure 4 is roughly 3 times larger than the 1.58 MHz peak in Figure 3. This change in intensity can in part be explained by the decrease in the coupling between Q_A^- and N_X. Such a decrease in A_{iso} would lead to a situation in which the nitrogen deviates significantly from the exact field cancellation condition of 2ν (^{14}N). The intensity of the ν_o, ν_-, and ν_+ peaks is maximal under exact field cancellation conditions, and any deviation from this will also lead to a decrease in the intensity of the ν_o, ν_-, and ν_+ peaks (*33*). We will show later that in *Synechocystis* the intensity of a peak near 1.5 MHz is quite variable. We cannot at this point assign the 0.58 and 0.85 MHz peaks of Figure 4, but we will demonstrate below that the 0.58 MHz peak most likely arises from the Q_A^-−N_Y coupling.

In summary we propose that in untreated and CN-treated Fe-intact spinach PS II centers, the semiquinone, Q_A^-, is magnetically coupled to two nearby nitrogens. One nitrogen, N_X, is clearly a peptide nitrogen of a nearby amino acid residue. The identity of the second nitrogen, N_Y, cannot be determined from the data in Figures 2−4. We propose that removal of the non-heme iron leads to a decrease in the isotropic hyperfine coupling between Q_A^- and the peptide nitrogen, N_X. This decrease in A_{iso} results in a loss of intensity of the ν_o, ν_-, and ν_+ peaks of N_X and a relative enhancement of the ESEEM peaks of the second nitrogen, N_Y. Comparison of the ESEEM spectra of CN-treated and Zn-repleted PS II centers in Figures 3 and 4 with the ESEEM spectra of the coupled Fe−Q_A^- PS II centers in Figure 2 clearly shows that the ESEEM peaks of the N_X and N_Y nitrogens are present in Figure 2. However, it is not readily apparent if the coupled Fe−Q_A^- ESEEM spectra most resemble the CN-treated PS II spectra (Figure 3) or the Zn-repleted spectra (Figure 4). Given that there is only a single peak near 0.75 MHz in Figure 2, we conclude that the CN treatment results in a quinone binding pocket most like that of the coupled Fe−Q_A^- pocket.

Astashkin et al. (*9*) have interpreted the ESEEM spectra of Q_A^- in Zn-substituted spinach PS II centers quite differently. They observe peaks at 0.88, 2.02, 2.88, and 5.0 MHz which they assign to a peptide nitrogen. However, they assign ESEEM peaks at 0.53, 0.88, 1.46, and 4.3 MHz to the ν_o, ν_+, and ν_{dq} transitions of an imidazole nitrogen ($e^2qQ = 1.5$ and $\eta = 0.9$) (*34*) of D2-His215 coupled to Q_A^- with $A_{iso} = 2.0$ MHz. Astashkin et al. did not observe a 0.85 MHz transition for this nitrogen and propose that the peak overlaps that of the ν_- peak of the peptide nitrogen. However, as we have mentioned, the intensity of the 1.46 MHz peak of the Zn-repleted spinach PS II particles has the same dependence on τ as does the 1.55 MHz peak of CN-treated spinach PS II particles in Figure 3A, suggesting that they represent the same nitrogen nucleus. Further, the difference in the line shape of the 4.35 MHz feature in Figure 4A as compared to the 4.75 MHz feature makes it tempting to assign the 4.35 MHz peak of the $\tau = 354$ ns and the 4.75 MHz peak of the $\tau = 213$ ns spectra to the transitions of different nitrogen nuclei coupled to Q_A^-. However, this difference in line shape is not present in Figure 4B, which shows the Zn−Q_A^- ESEEM spectra at $H = 3902$ G. This last result suggests that the line shape of the 4−5 MHz region in Figure 4 arises entirely from the splitting of the ν_{dq} ESEEM peak of N_X as discussed above for Figure 3 and by Deligiannakis et al. (*11*).

A recent study by Spoyalov et al. (*10*) indicates that the ESEEM spectra of Q_A^- in Zn-substituted reaction centers of purple photosynthetic bacteria are very similar to the spectra in Zn-repleted spinach PS II membranes (see Figure 4 and ref *9*). In their study of Q_A^- in Zn-substituted bacterial reaction centers, Spoyalov et al. (*10*) observe ESEEM peaks at 0.64, 0.85, 1.0, 1.46, 1.8, 2.78, and 4.2 MHz. They assign the spectrum as resulting from the coupling of Q_A^- to a peptide and a histidine nitrogen. However, they do not observe separate peaks for the peptide and histidine nitrogens and conclude that these peaks overlap. They calculate isotropic hyperfine couplings for the peptide and histidine nitrogens of 1.1 and 2.0 MHz, respectively. While we do not agree with the assignment of the histidine nitrogen coupling, this analysis supports our assertion that the removal of the non-heme iron can result in a ν_{dq} near 4.3 MHz for the peptide nitrogen.

Astashkin et al. (*9*) propose that the histidine nitrogen is from D2-His 215 and that the peptide nitrogen is from D2-Ala260. These two residues are thought to be hydrogen bonded to the O4 and O1 oxygens of Q_A^-, respectively. This is a reasonable model based on the proposed homology between PS II and the known structure of the photosynthetic reaction center of purple bacteria. However it is important to directly correlate the observed ESEEM peaks with particular amino acid residues. Such assignments require extensive isotopic labeling and mutagenesis of the residues likely to contribute to ESEEM spectra of Q_A^-. We have begun to perform such experiments on PS II core complexes isolated from *Synechocystis*.

Synechocystis Core Particles. One distinct advantage of using the cyanobacterium *Synechocystis* is that it is capable of taking up specific amino acids from its growth media and incorporating them into its proteins preferentially over residues synthesized de novo (*35*). This feature allows for the specific isotopic labeling of amino acids. We have successfully used this technique to identify a histidine ligand to the manganese cluster of the oxygen-evolving complex of PS II (*27*). More recently, we have used isotopic labeling to demonstrate that the tyrosine radical $Y_D^\bullet$ forms a hydrogen bond with the τ nitrogen of the D2-His189 amino acid residue (*36*). A second advantage of *Synechocystis* over spinach is the ability to perform genetic manipulations of the PS II centers in *Synechocystis*. Figure 5 compares the 3P-FT-ESEEM spectra of Q_A^- in CN-treated core particles at pH 9.2, 7.8, and 6 (traces a, b, d, and e). Trace c is the ESEEM spectrum of Q_A^- in untreated core particles at pH 7.8 passed through a hydroxylapatite column, which results in the decoupling of the electron spins of the iron and quinone spins (*12*). All five spectra compare well with the Fe-intact spinach spectra in Figures 1 and 2. Peaks are present in all five spectra at 0.7, 2.0, and 2.85 MHz. Traces a and b clearly show the dependence of the 4−5 MHz peak on the value of τ as was discussed above for Figure 3. The peak is at 5.0 MHz in trace a ($\tau = 213$ ns) and at 4.4 MHz in trace b ($\tau = 354$ ns). These peaks can easily be assigned to the peptide nitrogen N_X, discussed above. The two additional peaks at 1.55 and 3.6 MHz can be assigned to the second nitrogen N_Y. Comparison of traces c and d shows that the absence of the CN^- ligand to the non-heme iron leads to increases in the intensity of the 0.6, 2.2, and 3.6 MHz features. These

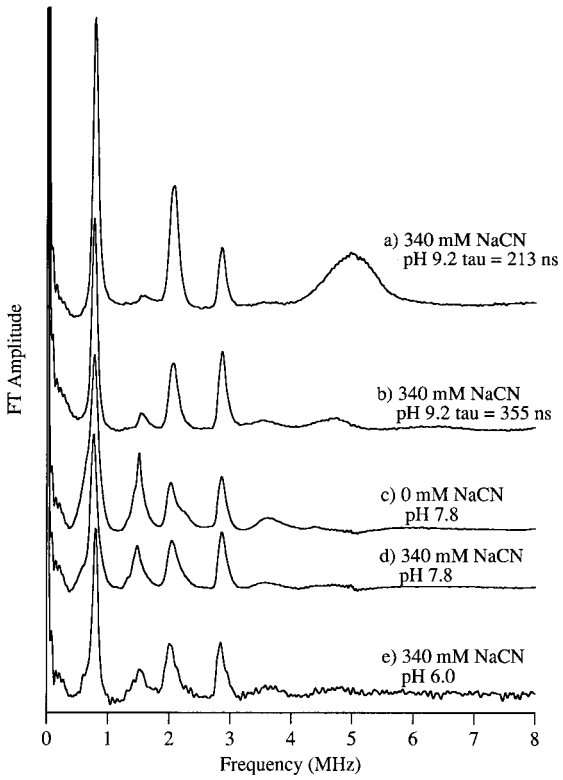

FIGURE 5: Comparison of three-pulse Fourier transform ESEEM spectra for Q_A^- in *Synechocystis* PS II centers (a) treated with 340 mM NaCN at pH 9.2, other experimental conditions, $\nu = 9.30$ GHz, $H = 3316$ G, $T = 20$ K, and $\tau = 213$ ns; (b) same as (a) except $\tau = 355$ ns; (c) treated with 340 mM NaCl at pH 7.8 and passed through a hydroxylapatite column, experimental conditions, $\nu = 9.29$ GHz, $H = 3312$ G, $T = 20$ K, and $\tau = 354$ ns; (d) same as (c) except treated with 340 mM NaCN; (e) treated with 340 mM NaCN at pH 6.0, experimental conditions, $\nu = 9.36$ GHz, $H = 3340$ G, $T = 20$ K, and $\tau = 351$ ns. For (a)−(e) microwave paper 50 W, $\pi/2$ pulse = 10 ns.

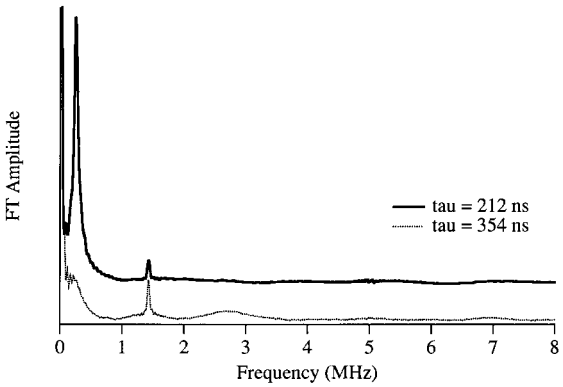

FIGURE 6: Three-pulse Fourier transform ESEEM spectra of Q_A^- in ^{15}N globally labeled *Synechocystis* at $\tau = 212$ and 354 ns. The experimental conditions are $\nu = 9.29$ GHz, microwave paper 50W, $\pi/2$ pulse = 10 ns, $H = 3312$ G, and $T = 20$ K.

data would suggest that the 0.6 and 2.2 MHz features as well as the 1.5 and 3.6 MHz peaks are due to the Q_A^-−N_Y coupling and that the contribution of these peaks to the ESEEM spectrum of Q_A^- is sensitive to perturbations of the non-heme iron site.

Figure 6 compares the ESEEM spectra, at two different values of τ, of Q_A^- in untreated PS II core particles of *Synechocystis* grown on a global ^{15}N medium. These results are consistent with our previously published report on ^{15}N-labeled CN-treated *Synechocystis* PS II centers at pH 9.2 and the previously published experiments on CN-treated spinach PS II membranes at pH 8.0 by Deligiannakis et al. (*8*). These similarities suggest conclusions drawn from experiments on in untreated PS II centers are also valid for assigning the ESEEM spectrum of in CN-treated BBY membranes.

The complete change in the ESEEM spectra demonstrates that the peaks in Figures 1−5 do truly arise from nitrogen nuclei. Three peaks are observed in Figure 6 at 0.28, 1.46, and 2.8 MHz. The peak at 1.46 MHz is at the free nuclear Larmor frequency of ^{15}N and represents one or more nitrogens weakly coupled to the quinone. Further, if the ESEEM spectrum is measured at 3690 G, the 1.46 MHz peak shifts to 1.5 MHz, which is the nuclear Larmor frequency of ^{15}N at 3690 G. This assignment contradicts a prior assignment by Deligiannakis et al. (*8*). In their experiments at a field of 3443 G, the free nuclear Larmor frequency of ^{15}N is 1.48 MHz. Although they observe an ESEEM peak near 1.5 MHz, they do not assign it to ^{15}N. They subsequently conclude that, since a 1.5 MHz peak was present in both an ^{14}N global and an ^{15}N global spectrum, it must arise from a nucleus other than nitrogen and conclude that Q_A^- is coupled to only one nitrogen nuclei. Our data at two different field values convincingly show that Q_A^- must be coupled to at least two nitrogen nuclei.

The intensity of ESEEM peaks for an $I = {}^1/_2$ nucleus, such as ^{15}N, in a 3P-ESEEM spectrum has a very specific dependence on τ, the interval between the first and second microwave pulses of the three-pulse experiments. If τ is chosen to be equal to $1/\nu_-$ then the intensity of the ν_+ peak is minimized. Conversely, if τ is chosen to be equal to $1/\nu_+$ then the intensity of the ν_- peak is minimized. For example, if the 0.28 and 2.8 MHz peaks truly represent the $\nu_\pm$ transitions of an ^{15}N nucleus, then the 0.28 MHz peak should be suppressed at a $\tau = 1/(2.8\ \text{MHz})$ or 357 ns. From Figure 6, it is clear that the 0.28 peak is absent from the $\tau = 354$ ns spectrum. This τ suppression demonstrates that the 0.28 and 2.8 MHz peaks are indeed the $\nu_\pm$ transitions of a single class of nucleus.

Lai et al. (*37*) have shown that when $A_{iso} = 2\nu(^{15}N)$, that is, near exact field cancellation, the ESEEM spectrum of the ^{15}N nucleus has two peaks at $3A_{dip}/4$ and $2\nu(^{15}N)$. For the 0.28 and 2.8 MHz features, these expressions then yield hyperfine constants of A_{iso} 2.8 and A_{dip} 0.37 MHz. The corresponding parameters would be scaled by the ratio of the magnetic moments of the ^{14}N and ^{15}N nuclei.

$$A_{iso}(^{14}N) = A_{iso}(^{15}N)\,\frac{\gamma(^{14}N)}{\gamma(^{15}N)} = 2.0\ \text{MHz} \qquad (3)$$

It is thus clear that the 0.26 and 2.7 MHz peaks in Figure 6 arise from the Q_A^-−N_X peptide nitrogen coupling. We can estimate the O−N hydrogen bond distance from the dipolar coupling using the equation $A_{dip} = \mu_{Q_A}\mu_N\rho_O/r^3$, where μ_{Q_A} is the electron magnetic moment of the radical, μ_N is the nuclear magnetic moment of the peptide nitrogen, and ρ_O is the unpaired spin density on the quinone oxygen. Assuming $\rho_O = 0.208$ (*7*), the O−N hydrogen bond would be would be approximately 2.0.

From Figure 6, it is clear that no ESEEM detectable nitrogen is coupled to Q_A^- with an A_{iso} between 0 and 2.8

MHz. To verify this conclusion, we performed Mims ENDOR experiments on ^{15}N-*Synechocystis* PS II at pH 7.8 isolated using a hydroxylapatite column. Campbell et al. (*36*) successfully used Mims ENDOR to observe the 0.8 MHz coupling between $Y_D^{\bullet}$ and the τ nitrogen of D2-His189 in PS II centers. If couplings of this magnitude are present in the Q_A^- system, we should be able to observe them with ENDOR spectroscopy. However, in our Mims ENDOR spectra of Q_A^- we only observe ENDOR peaks near 1.46 and 2.8 MHz (data not shown). The full width at half-maximum of the 1.46 MHz was approximately 0.2 MHz. Given the sharpness of the 0.28 MHz peak, it would be reasonable to conclude that, if a second nitrogen were coupled to Q_A^- with an A_{iso} near 2.0 MHz, a second peak near 0.28 MHz would be detectable unless this second nitrogen had an A_{iso} and an A_{dip} identical to that of N_X, an unlikely coincidence. We can now assign the N_Y nitrogen as a weakly coupled nitrogen with $A_{iso} < 0.2$ MHz.

D2-Ala260. Although previous experimenters (*8, 9, 16, 17*) have assigned the 0.7, 2.0, 2.85, and 5.0 MHz peaks to the peptide nitrogen of D2-Ala260, no genetic or isotopic labeling experiments have been previously performed to confirm this assignment. The simplest way to determine the contribution of D2-Ala260 would be to selectively label the peptide nitrogen of this residue with ^{15}N and observe which peaks in the ESEEM spectrum of Q_A^- disappear. To this end, PS II centers were isolated from *Synechocystis* grown on a media containing $^{14}NO_3^-$ and ^{15}N alanine. As only the alanine peptide nitrogen will be ^{15}N in these samples, any peaks which disappear can be assigned to an alanine peptide nitrogen. Figure 7A compares the ESEEM spectrum of Q_A^- in $^{15}N^-$ alanine with the ESEEM spectrum of natural abundance ^{14}N-*Synechocystis*. For N nuclei coupled to Q_A^-, each nuclei will contribute a time domain spectrum, $S(3P)_i$, where i indicates a particular nucleus. Mims (*38*) has shown that the total observed time domain three-pulse ESEEM spectrum, $S(3P)_{tot}$, is given by

$$S(3P)_{tot} = \prod_{i=1}^{N} S(3P)_i \qquad (4)$$

Therefore, if one divided the S(^{14}N-global) time domain spectrum by the S(^{15}N-ala:^{14}N-background) time domain spectrum, the resulting time domain spectrum would contain only contributions from nitrogens belonging to ^{14}N-alanine residues. The Fourier transform of this divided or "ratioed" time domain would then be the frequency domain ESEEM spectrum of the ^{14}N−Ala nitrogens coupled to Q_A^-.

Figure 7B shows the ratioed spectrum for the data in Figure 7A. The ratioed spectrum shows positive peaks at 0.6, 0.8, 1.5, 2.2, and 2.8 MHz. The two positive peaks at 1.5 and 2.2 MHz can easily be assigned to ^{14}N−Ala nitrogen transitions. While there is a positive peak near 0.8, this feature may represent a small change in the line shape of the very intense 0.75 MHz peak between the two samples. However, it is equally possible that the positive peak near 0.8 does indeed represent an ^{14}N−Ala nitrogen peak. It is clear from Figure 7A that the entire 1.5 MHz peak did not disappear upon isotopic labeling. Given that 70% of the ^{15}N-substituted alanine is incorporated, this attenuated effect suggests that a third class of nitrogens may be weakly coupled to Q_A^-.

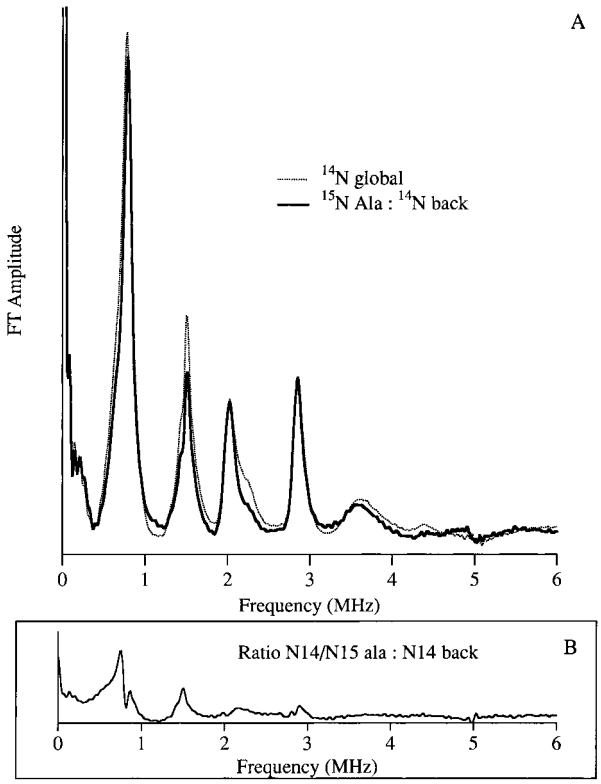

FIGURE 7: (A) Comparison of three-pulse Fourier transform ESEEM spectra of Q_A^- in *Synechocystis* untreated PSII centers which contain natural abundance ^{14}N- and globally ^{15}N-labeled alanine amino acid residues. (B) Fourier transform of the ratio of the corresponding time domains of the data in panel A. The experimental conditions are $\nu = 9.29$ GHz, microwave paper 50 W, $\pi/2$ pulse = 10 ns, $H = 3315$ G, $T = 20$ K, and $\tau = 354$ ns.

We conclude that an alanine peptide nitrogen is coupled to Q_A^- and has an ESEEM spectrum consisting of peaks at 1.5 and 2.2 MHz and possibly at 0.6−0.8 MHz. We had proposed in the discussion of the spinach PS II ESEEM spectrum that the 1.5 MHz peak represents the Q_A^-−N_Y coupling. We can now conclude that the N_Y nitrogen is the peptide nitrogen of an alanine residue. These are the same peaks which we showed were affected by the ligation of CN^- to the non-heme iron of *Synechocystis*. We can conclude also that the N_X peptide nitrogen is not from alanine. If N_X was an alanine peptide nitrogen, we would observe a positive peak near 2.7 MHz (see $\tau = 354$ ns trace of Figure 6). No such peak is present in Figure 6.

To confirm our alanine isotopic labeling experiments, we isolated PS II centers from the mutant D2-Ala 260 to D2-Gly260 grown on an $^{14}NO_3^-$ medium containing ^{15}N-glycine. Figure 8A compares the ESEEM spectrum of ^{14}N global Q_A^- and ^{15}N-Gly Q_A^- and Figure 8B shows the ratioed spectrum. The ratioed spectrum shows only significant positive peaks near 0.6, 1.45, and 2.2 MHz. While the spectral changes at 0.6 and 1.45 MHz are more pronounced in Figure 8 than they were in Figure 7 for the alanine data, a significant portion of the 1.45 MHz peak remains upon labeling. As we concluded for the alanine substitution data, this remaining intensity suggests a third class of nitrogens weakly coupled to Q_A^-. On the basis of the actual change in the intensity of the 1.45 MHz peak upon glycine labeling, we can conclude that a glycine peptide nitrogen is coupled to Q_A^-. Because residue D2−260 is the only common factor in the ^{15}N-alanine

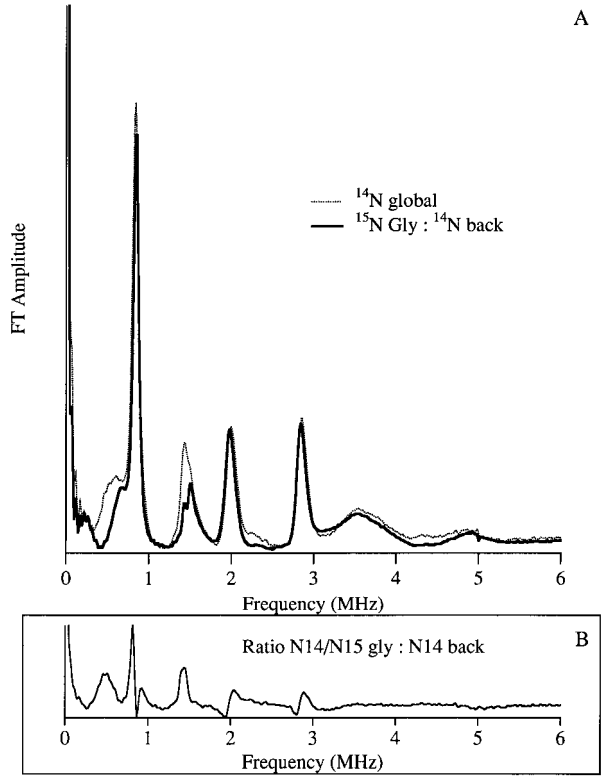

FIGURE 8: (A) Comparison of three-pulse Fourier transform ESEEM spectra of Q_A^- in untreated *Synechocystis* PSII centers in which D2-Ala260 is changed to glycine and which contain natural abundance ^{14}N- and globally ^{15}N-labeled glycine amino acid residues. (B) Fourier transform of the ratio of the corresponding time domains of the data in panel A. The experimental conditions are $\nu = 9.29$ GHz, microwave paper 50 W, $\pi/2$ pulse = 10 ns, $H = 3315$ G, $T = 20$ K, and $\tau = 354$ ns.

and ^{15}N-glycine isotopic labeling experiments shown in Figures 7 and 8, it can be concluded that the peptide nitrogen of this residue is coupled to Q_A^- and has nuclear transition frequencies at approximately 0.6, 1.5, and 2.2 MHz.

D2-His215. As discussed above, a histidine residue has been proposed to be magnetically coupled to Q_A^- in Zn-repleted spinach PS II centers (*9*). However, in a prior publication (*12*), we used isotopic labeling to show that the ESEEM spectrum of Q_A^- in *Synechocystis* PS II centers has no features which can be assigned to a coupling between Q_A^- and histidine. We can conclude that there is no strong magnetic coupling between and the imidazole nitrogen of a histidine residue. We can also conclude that N_X is not the peptide nitrogen of a histidine residue.

D2-Trp253. Another nearby nitrogen containing residue is D2-Trp 253. Figure 9 compares the three-pulse ESEEM spectrum of Q_A^- in wild type *Synechocystis* and in two mutants in which D2-Trp 253 has been changed to a tyrosine and a phenylalanine. Both mutations show changes at 0.6, 1.5, and 2.2 MHz with the Trp to Tyr showing the largest change. These data suggest that the mutation in some manner affects the coupling of the quinone to the peptide nitrogen of D2-Ala260. Given the similarity in the ESEEM spectra for the wild type and Trp to Phe mutant, it seems likely that the hydroxyl group of the tyrosine results in a perturbation of the quinone binding pocket. While these mutations lead to large changes in the intensities of some of the ESEEM peaks in Figure 9, they do not lead to the elimination of any

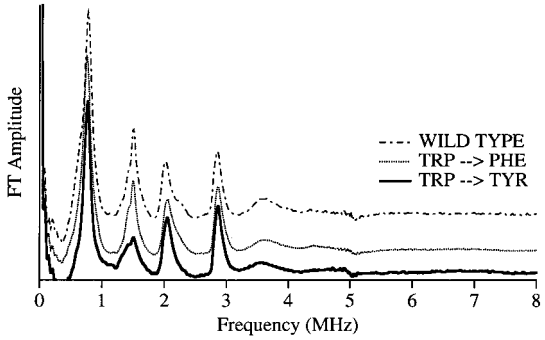

FIGURE 9: Comparison of 3P−FT-ESEEM spectra of Q_A^- in wild type and PS II centers in which residue D2-Trp253 has been changed to either phenylalanine or tyrosine. The wild-type experimental conditions are $\nu = 9.29$ GHz, microwave paper 50 W, $\pi/2$ pulse = 10 ns, $H = 3315$ G, and $\tau = 355$ ns. The phenylalanine and tyrosine mutation experimental conditions are $\nu = 9.30$ GHz, microwave paper 50 W, $\pi/2$ pulse = 10 ns, $H = 3323$ G, and $\tau = 353$ ns.

ESEEM peaks. It can be concluded that the ring nitrogen of residue D2-Trp253 does not contribute directly to the ESEEM spectrum of Q_A^-. On the basis of similar experiments in bacterial reaction centers, Spoyalov et al. came to the same conclusion (*10*).

DISCUSSION

Models of the Q_A binding site of PS II have predicted that the O1 and O4 oxygens of the quinone are hydrogen bonded to the peptide nitrogen of D2-Ala260 and to the imidazole nitrogen of D2- His215 (*1*−*3*). The proximity of Q_A^- to these ^{15}N nuclei suggests that the $I = 1$ nuclear spin would be magnetically coupled to the electron spin Q_A^-. We have demonstrated that in PS II centers isolated from *Synechocystis*, Q_A^- is magnetically coupled to the peptide nitrogen of D2-Ala260, though not as previously assigned (*8, 9, 13, 16, 17*). Furthermore, we observe no evidence for a coupling to the imidazole nitrogen of D2-His215. Instead, we observe a coupling between Q_A^- and a second peptide nitrogen N_X, of unknown origin. We propose that in Fe-intact spinach PS II membranes these same two nitrogens are coupled to Q_A^-.

An important issue is what, if any, relevance do these conclusions derived from Fe-intact but decoupled PS II centers have on the assignment of the ESEEM spectra of Q_A^- in Fe-depleted and Zn-repleted spinach PS II membranes. Comparison of the Zn-repleted spectra in Figure 4 with the native high-spin iron spectra in Figure 2 clearly shows that the removal of the non-heme iron results in a perturbation of the magnetic interactions that Q_A^- makes with nearby nuclei. It is clear that Figure 2 does not contain the 0.58 and 0.8 MHz peaks present in Figure 4, which others assign to a histidine−Q_A^- coupling (*9*). It is therefore not unreasonable to expect that, in iron-containing PS II centers, a quinone−histidine coupling is absent, but that the removal of the iron leads to such an interaction. Such a proposal is the opposite of one proposed by Kawamori et al., who postulate that CN^- ligation results in the loss of a prexisting histidine−quinone hydrogen bond (*16*). Many researchers have documented a variability in the intensity of 0.6, 0.8, and 1.46 MHz peaks depending on sample conditions (*10, 13, 16*).

In our study of the ESEEM spectrum of Q_A^- in *Synechocystis* PS II centers, we have established that the intensities of the ESEEM peaks of D2-Ala260 are also quite variable. We have further shown that the frequency of an ESEEM peak of the N_Y nitrogen may vary from 1.45 to 1.58 MHz. As mentioned above, the intensity of these 1.45−1.58 MHz peaks has the same dependence on τ as the 1.46 MHz peak of the Zn-repleted spinach PS II membranes. These correlations strongly suggest that the peptide nitrogen of D2-Ala260 is the source of the 0.6, 0.85, and 1.46 MHz peaks present in the ESEEM spectrum of Fe-depleted and Zn-repleted spinach PS II membranes. In many respects the large variability observed in the intensity of these peaks is more consistent with a weakly hydrogen bonded D2-Ala260 peptide nitrogen than with a strongly hydrogen bonded imidazole nitrogen of D2-His215. However, until isotopic substitution experiments similar to the ones presented in Figures 6−8 are performed on Zn-substituted PS II centers, our assignment of the ESEEM spectra of Q_A^- in Zn-repleted PS II remains in doubt.

Our lack of observation of a histidine−quinone coupling in Fe-intact PS II centers does not mean that a hydrogen bond does not exist between an imidazole nitrogen of D2-His215 and Q_A^-. The intensity of ESEEM peaks of an ^{14}N nucleus is a delicate interplay of the nuclear Zeeman, hyperfine coupling, and quadrupole interaction terms of the spin Hamiltonian. We suggested above that a third nitrogen nucleus might be contributing to the ESEEM peak near 1.5 MHz. We know from Figure 6 that this third nucleus can only be weakly coupled to Q_A^-. This third nucleus may be D2-His215, but given the spectral congestion brought about by the ESEEM peaks of N_X and D2-Ala260, it is possible that any contribution from D2-His215 is obscured and its observation simply awaits the proper combination of isotopic substitution and site-directed mutagenesis to bring it to the forefront as we did for the D2-Ala260 peptide nitrogen. Furthermore, our inability to find direct experimental evidence for a Q_A^-−histidine coupling in PS II centers should not be interpreted as evidence that the binding site in PS II is different from the binding site in photosynthetic purple bacterial reaction centers. There is in fact a great similarity between the ESEEM spectra of Q_A^- in the bacterial system and PS II, as has been pointed by others (*10*, *11*). This spectral similarity implies that the binding site of in PS II does indeed resemble the binding site in the bacterial system more than it differs.

The large isotropic hyperfine coupling between Q_A^- and N_X, $A_{iso} = 1.8$ MHz, demonstrates significant delocalization of the electron spin density of Q_A^- onto the N_X peptide nitrogen and indicates the presence of a hydrogen bond between Q_A^- and N_X (*36*). In a like manner, the weak coupling, $A_{iso} \cong 0$ MHz, between Q_A^- and D2-Ala260 indicates that there is little delocalization of the electron spin density onto this peptide nitrogen and indicates a weak hydrogen bond between Q_A^- and D2-Ala260. FT-IR (*5*, *6*) and Q-band CW-EPR (*7*) experiments have shown that the O4 oxygen of Q_A^- participates in a strong hydrogen bond but that the O1 oxygen does not participate in a hydrogen bond. These data would suggest that N_X is hydrogen bonded to O4 and that D2-Ala260 is close to O1. The proximity of the O1 oxygen and D2-Ala260 peptide nitrogen is already suspected on the basis of the X-ray structure of the bacterial center (*2*, *3*).

In summary, we have performed a series of ESEEM experiments on Q_A^- in Fe-intact PS II centers isolated from isotopically labeled wild type and site-directed mutants of *Synechocystis*. We demonstrate that, in Fe-intact PS II centers, Q_A^- is magnetically coupled to two nearby peptide nitrogens, D2-Ala260 and one as yet unidentified. We show that D2-Ala260 is weakly coupled to Q_A^- with ESEEM peaks near 0.6, 1.46, and 2.2 MHz. We show that the second peptide nitrogen, N_X, is strongly coupled to Q_A^- with ESEEM peaks at 0.75, 2.0, 2.85, and 4−5 MHz. It is quite likely that this nitrogen is responsible for the strong hydrogen bond to the O4 oxygen of Q_A, which was predicted by FT-IR (*5*, *6*) and Q-band CW-EPR (*7*) experiments. In previous assignments of the ESEEM spectra (*8*−*11*, *13*, *16*) this strongly coupled nitrogen was assigned to D2-Ala260, but we report strong evidence that it is not D2-Ala260. We further show that neither the imidazole and peptide nitrogens of histidine nor the ring nitrogen of D2-Trp253 contributes to the ESEEM spectra of Q_A^- in Fe-intact but decoupled PS II centers. We also argue that histidine is not coupled to Q_A^- in Zn-substituted PS II centers and bacterial reaction centers and that the peaks assigned to this histidine coupling are due to the Q_A^-−D2-Ala260 coupling. However, this final assignment awaits confirmation through isotopic labeling of Zn-substituted reaction centers.

REFERENCES

1. Diner, B. A., and Babcock, G. T. (1996) in *Oxygenic Photosynthesis: The Light Reactions* (Ort, D., and Yocum, C., Eds.) p 213, Kluwer Academic Publishers, Dordrecht, The Netherlands.
2. Komiya, H., Yeates, T. O., Rees, D. C., Allen, J. P., and Feher, G. (1988) *Proc. Natl. Acad. Sci. U.S.A. 85*, 9012.
3. Michel, H., and Deisenhofer, J. (1988) *Biochemistry 27*, 1.
4. Diner, B. A., Petrouleas, V., and Wendoloski, J. J. (1991) *Physiol. Plant. 81*, 423.
5. Brudler, R., de Groot, H. J. M., van Liemt W. B. S., Steggerda, W. F., Esmeijer, R., Gast, P., Hoff, A. J., Lugtenburg, J., and Gerwert, K. (1994) *EMBO J. 13*, 5523.
6. Breton, J., Boullais, C., Burie, J. R., Berger, G., Nabedryk, E., and Mioskowski, C. (1994) *Biochemistry 33*, 14378.
7. Isaacson, R. A., Abresch, E. C., Lendzian, F., Boullais, C., Paddock, M. L., Mioskowski, C., Lubitz, W., and Feher, G. (1996) in *The Reaction Center of Photosynthetic Bacteria: Structure and Dynamic* (Michel-Beyerle, M.-E., Ed.) p 353, Springer, New York.
8. Deligiannakis, Y., Boussac, A., and Rutherford, A. W. (1995) *Biochemistry 34*, 16030.
9. Astashkin, A. V., Kawamori, A., Kodera, Y., Kuroiwa, S., and Akabori, K. (1995) *J. Chem. Phys. 102*, 3383.
10. Spoyalov, A. P., Hulsebosch, R. J., Shochat, S., Gast, P., and Hoff, A. J. (1996) *Chem. Phys. Lett. 263*, 715.
11. Bosch, M. K., Gast, P., Hoff, A. J., Spoyalov, A. P., and Tsvetkov, Yu. D. (1994) *Chem. Phys. Lett. 239*, 306.
12. Tang X.-S., Peloquin, J. M., Lorigan, G. A., Britt, R. D., and Diner, B. A. (1995) in *Photosynthesis: From Light to Biosphere* (Mathis, P., Ed.) Vol. 1, p 775, Kluwer Academic Publishers, Dordrecht, The Netherlands.
13. MacMillan, F., Kurreck, J., Adir, N., Lendzian, F., Kass, F., Reifarth, F., Renger, G., and Lubitz, W. (1995) in *Photosynthesis: From Light to Biosphere* (Mathis, P., Ed.) Vol. 1, p 659, Kluwer Academic Publishers, Dordrecht, The Netherlands.
14. Klimov, V. V., Dolan, E., Shaw, E. R., and Ke, B. (1990) *Proc. Natl. Acad. Sci. U.S.A. 77*, 9012.

15. Rutherford, A W., and Zimmerman, J. L. (1992) *Biochim. Biophys. Acta 767*, 168.
16. Kawamori, A., Mino, H., Astashkin, A. V., Kuroiwa, S., and Akabori, K. (1995) in *Photosynthesis: From Light to Biosphere* (Mathis, P., Ed.) Vol. 1, p 563, Kluwer Academic Publishers, Dordrecht, The Netherlands.
17. Deligiannakis, Y., Jegerschöld, C., and Rutherford, W. A. (1997) *Chem. Phys. Lett. 270*, 564.
18. MacMillan, F., Lendzian, F., Renger, G., and Lubitz, W. (1995) *Biochemistry 34*, 8144.
19. Rigby, S. E. J., Heathcote, P., Evans, M. C. W., and Nugent, J. H. A. (1995) *Biochemistry 34*, 12075.
20. Butler, W. F., Cavlo, R., Fredkin, D. R., Isaacson, R. A., Okamura, M. Y., and Feher, G. (1984) *Biophys. J. 45*, 947.
21. Sanakis, Y., Petreouleas, V., and Diner, B. A. (1994) *Biochemistry 33*, 9922.
22. Deisenhofer, J., and Michel, H. (1989) *EMBO J. 8*, 2149.
23. Berthold, D. A., Babcock, G. T., and Yocum, C. F. (1981) *FEBS Lett. 134*, 231.
24. Campbell, K. A., Gregor, W., Pham, D. P., Peloquin, J. M., Debus, R. J., and Britt, R. D. (1998) *Biochemistry 37*, 5039.
25. Tang, X. S., and Diner, B. A. (1994) *Biochemistry 33*, 4594.
26. Rippka, R., Deruelles, J., Waterbury, J. B., Herdman, M., and Stanier, R. (1979) *J. Gen. Microbiol. 111*, 1.
27. Tang, X.-S., Diner, B. A., Larsen, B. S., Gilchrist, M. L., Lorigan, G. A., and Britt, R. D. (1994) *Proc. Natl. Acad. Sci. U.S.A. 91*, 704.
28. Rögner, M., Nixon, P. J., and Diner, B. A. (1990) *J. Biol. Chem. 256*, 6189.
29. Koulougliotis, D., Tang, X. S., Diner, B. A., and Brudvig, G. W. (1995) *Biochemistry 34*, 2850.
30. Sturgeon, B. E., and Britt, R. D. (1992) *Rev. Sci. Instrum. 63*, 2187.
31. Mims. W. B. (1984) *J. Magn. Reson. 59*, 291..
32. Nixon, P. J., Rögner, M., and Diner, B. A. (1991) *Plant Cell 3*, 383.
33. Flanagan, H. L., and Singel, D. J. (1987) *J. Chem. Phys. 87*, 5606.
34. Edmonds, D. T. (1977) *Phys. Rev. C: Nucl. Phys. 29*, 233.
35. Diner, B. A. (1999) Photosynthesis: Molecular Biology of Energy Capture in *Methods in Enzymology* (McIntosh, L., Ed.) Vol. 297, Academic Press, San Diego, CA (in press).
36. Campbell, K. A., Peloquin, J. M., Diner, B. A., Tang, X. S., Chisholm, D. A., and Britt, R. D. (1997) *J. Am. Chem. Soc. 119*, 4787.
37. Lai, A., Flanagan, H. L., and Singel, D. J. (1988) *J. Chem. Phys. 89*, 7161.
38. Mims, W. B., Davis, J. L., and Peisach, J. (1990) *J. Magn. Reson. 86*, 273.

BI982033L